ASM Sc. J., 15, 2021

https://doi.org/10.32802/asmscj.2021.592

Verification of Human Lumbar Vertebrae and Intervertebral Disc Finite Element Models under Mechanical Forces

Mohankumar Palaniswamy[1*], Anis Suhaila Shuib[1], Ng Khai Ching[2] and Shajan Koshy[3]

[1]*School of Engineering, Taylor's University, Malaysia*

[2]*School of Engineering, Nottingham University, Malaysia*

[3]*School of Medicine, Taylor's University, Malaysia*

Bone, being nonhomogeneous in nature need a complicated and time-consuming process to undergo computed simulation like finite element analysis. To overcome this hurdle, assuming a nonhomogeneous model as homogeneous could be a solution. The objective of this study is to focus on developing a homogeneous human lumbar finite element models and verify them under mechanical force by measuring disc stress, disc strain, disc deformation, total strain, and total deformation. Experimental and geometrical analysis were performed before verifying the lumbar model. To verify the models' reliability, nonhomogeneous lumbar models were also developed. Five different static structural simulations were performed on four lumbar segments, and twenty parameters were measured. Numerically, out of twenty, eighteen parameters showed very less or no significant difference between homogeneous and nonhomogeneous models of the intervertebral discs and lumbar vertebrae. At the same time, proper caution to be provided while examining the results. With this validation procedure, researchers can process artifact images to get more information which enables them to contribute to the patient's well-being.

Keywords: homogeneous; validation; lumbar vertebra; IVD; FEA; mechanical

I. INTRODUCTION

A structure or a body made from the same material or element in all directions is termed as Homogeneous (H), for example, glass and wood. Materials that have the same properties in all the directions are termed Isotropic, for example, glass. Whereas, materials with different properties in different directions are termed as Anisotropic, for example, wood and bone. Generally, bone is considered as an anisotropic nonhomogeneous model. The shaft of a long bone like femur has longitudinal Young's modulus of 9.15 ± 5.98 GPa in static and 11.05 ± 3.46 Gpa in dynamic. Whilst, in latitudinal, it is 3.05 ± 1.14 GPa in static and 8.3 ± 3.25 GPa in dynamic (Weerasooriya *et al.*, 2016).

While running a Finite Element Analysis (FEA), the structure and material properties play a vital role. A patient-specific finite element model can be obtained through the CT scan. CT scan is a series of X-ray images taken at a regular interval like 0.2, 0.5, 1.0 mm. This series of images is called Digital Imaging and Communications in Medicine (DICOM) images (Pianykh, 2012). With a clear DICOM image, nonhomogeneous (NH) models can be easily developed. Whilst, when the DICOM images are filled with noises or artifacts caused because of metal implants, then it is very challenging to develop a nonhomogeneous model. In some surgical treatments like scoliosis correction, vertebrectomy, total replacement, a small portion or a part of the bone is removed, and it is substituted by a metal implant. When these patients with metal implants undergo a CT scan, X-rays from the CT scan gets refracted because of the metal implanted inside their body which results in noisy DICOM images.

Human bone is nonhomogeneous in nature. Both the bone and intervertebral disc (IVD) is made up of two layers. Bone

*Corresponding author's e-mail: mohanphysionix06@live.com

has an inner trabecular bone which is enclosed by an outer cortical bone. The outer thick white layer is cortical, and the inner is trabecular (refer to Figure 1(a)). Whereas, IVD has an inner fluid-like substance called nucleus pulposus which is covered by fibres called annular fibrosus (Erwin and Hood, 2014). Since post-operated patients have metal implants, the CT scan images have a lot of artifacts. Due to the artifacts, the exact layers of cortical and trabecular are unable to be distinguished (refer to Figure 1 (b)). It is highly impractical or unachievable at all to develop a proper nonhomogeneous 3D model from the DICOM images which are affected by artifacts and noises. On the other hand, developing a homogeneous model from DICOM images that are affected by artifacts and noises is still achievable (refer to Figure 1 (c)).

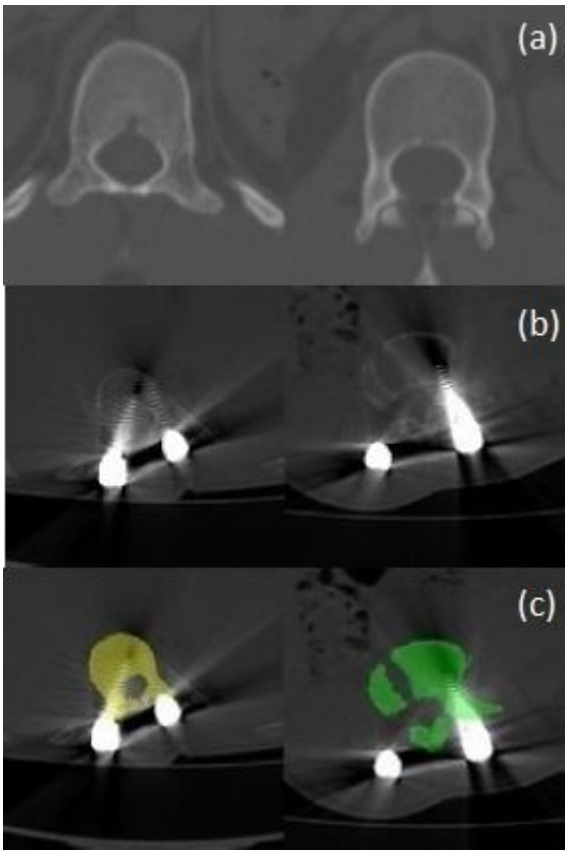

Figure 1. DICOM images of (a) normal, (b) post-operated with metal implants, (c) post-operated after image segmentation

Most of the prior bone FEA studies done had used an anisotropic nonhomogeneous model. At the same time, looking at the literature, isotropic homogeneous properties were used in several bone FEA studies, due to its convenience (Eswaran *et al.*, 2007; Zulkifi *et al.*, 2011; Shamnadh *et al.*, 2017). But their results were not validated. Using homogeneous lumbar models and isotropic material property, range of motion (ROM) of the human lumbar segment was alone validated in our previous study (Palaniswamy *et al.*, 2019). In this study, the same previously ROM validated human lumbar segments were used to validate the biomechanical properties like stress, strain, and deformation of the lumbar discs and lumbar vertebral segments. This type of validation procedure is convenient and helps the researchers to perform various research on the spine even if the images were affected with artifacts. These researches, in turn, help to develop a healthy society and better living as proposed in the global goals.

The literature review showed that several studies were done in the early days to find the mechanical strength of vertebra. Most of the studies used vertebrae from human cadavers and applied mechanical forces. Trexler *et al.*, (Trexler *et al.*, 2011) used a modified Split Hopkinson Pressure Bar (SHPB) to find shear loading in biological tissues. Bisschop *et al.*, (Bisschop *et al.*, 2013) found the torsional biomechanics of the spine which underwent lumbar laminectomy using Instron. Doulgeris *et al.*, (Doulgeris *et al.*, 2014) used Instron hydraulic apparatus to observe the effects of loading rate in axial rotation mechanics of the lumbar spine. Rahm *et al.*, (Rahm *et al.*, 2019) used MTS mini bionix hydraulic machine to determine the mechanical contribution of the intact rib cage during testing an instrumented specimen. All these studies mentioned above were conducted using human cadaver models.

Limitations to the cadaveric studies are numerous. IVDs in cadaver does not have the same physiological properties as *in vivo* due to lower fluid. It is also possible for the IVD to get damaged and show altered mechanics due to the presence of pressure sensors (Jones, 2013). Not only the IVD, but even vertebrae also face the same issues. Studies showed that approximately 2600 N is enough to cause failure or dislocation in the upper thoracic spine. However, a cadaver study reported that 613 N caused the failure (Oatis, 2016). Another study conducted by Hutton et al., on 58 lumbar samples between the age 17 to 65 years found that the load required to break lumbar vertebra ranges between 810 N to 15,559 N (Hutton *et al.*, 1979). Adding to these varying results, the preservation and maintenance of cadavers need

sophisticated lab features and most importantly, the availability of human cadaver. To build and maintain a lab, researchers need more fund. Not all researchers can afford it. Particularly, the issues with human cadaver access. At least the cadaver of normal human can be obtained easily. But there are certain disease and musculoskeletal structural disorders like kyphosis, scoliosis, lordosis which affect only two to three percent of the population. When a researcher wants to research scoliosis, which affects the structure of the spine, obtaining scoliosis affected cadaver is very rare or highly impossible. Hence, there is a need to find an alternate way to solve these cadaver issues. It could be the subject-specific finite element analysis. Using the patients CT or MRI scan data, a three-dimensional model of the bone or an organ can be developed digitally and subjected to simulation. With appropriate material properties and simulation procedures, finite element analysis can yield accurate results like experimental studies.

To develop a patient-specific finite element model, researchers need clear DICOM images. Whereas, in certain scenarios, patients are implanted with metal implants. These metal implants refract X-rays and produce artifacts or noisy DICOM images. These artifacts can be bypassed by considering the bone as a homogeneous model (Eswaran *et al.*, 2007; Zulkifi *et al.*, 2011; Shamnadh *et al.*, 2017). This paper presents the framework of considering a normal human vertebral segment as homogeneous and validate it by subjecting it to mechanical forces.

II. MATERIALS AND METHOD

After obtaining the ethical committee approval from the Human Ethics Committee, Taylor's University (HEC/2015/SOE/022), and data collection approval from the Dean of Madras Medical College (01108/MEI/2015), lumbar DICOM images of a normal young adult was obtained from the radiology department. The DICOM images were imported into Materialise version 20.0 (Materialise Inc., Belgium). Image segmentation was done and two separate masks were developed for lumbar vertebrae and IVD. It took nearly five hours to perform manual image segmentation. No muscles, ligaments, blood vessels, nerves, endplates, and metal implants were included in the modeling of lumbar segments. The developed masks were converted into parts. Parts were then smoothened and wrapped to cover tiny holes and sharp edges. An adaptive remesh was done with the triangle edge length of 1 mm to preserve surface contours. After performing a mesh independence study, a volume mesh was created using a four-node tetrahedral element with a maximum edge length of 2 mm. The 3D mesh models of four subject-specific homogeneous human lumbar segments L_1-L_2, L_2-L_3, L_3-L_4, and L_4-L_5 were developed and exported as .CDB files. The developed lumbar segments underwent geometrical analysis using Ansys Workbench version 17.2 (Ansys, Inc., U.S.A). The results of these analyses were found to be reliable. Very detailed explanations of the experimental analysis and geometrical analysis are presented in the previous study (Palaniswamy *et al.*, 2019). The same four homogeneous human lumbar segments were used in this study as well.

Table 1. Geometrical properties

Lumbar Segments	Homogeneous			
	Volume	**Mass (Kg)**	**Nodes**	**Elements**
L_1-L_2	85.62 cm^3	0.6721	56125	320425
L_2-L_3	95.93 cm^3	0.753	62596	358597
L_3-L_4	100 cm^3	0.785	65286	375760
L_4-L_5	114.50 cm^3	0.8125	68262	394379
Lumbar Segments	**Nonhomogeneous**			
	Volume	**Mass (Kg)**	**Nodes**	**Elements**
L_1-L_2	85.62 cm^3	0.6721	59235	341076
L_2-L_3	95.93 cm^3	0.753	72233	388263
L_3-L_4	100 cm^3	0.785	78661	427263
L_4-L_5	114.50 cm^3	0.8125	83261	498218

After performing the experimental analysis and geometrical analysis, validation analysis of homogeneous finite element models of lumbar vertebrae is performed. Linear homogeneous isotropic material properties were used for the validation of lumbar finite element models. This supposition was verified by developing nonhomogeneous lumbar segments for the same subject with sperate material properties for trabecular bone, cortical bone, nucleus pulposus, and annular fibrosus. Both the volume and mass of the models were the same in both the homogeneous and nonhomogeneous, but the number of nodes and elements were different. The geometrical properties of the homogeneous and nonhomogeneous models are presented in below Table 1. Material properties were assigned which were

acquired from the works of literature (Li and Wang, 2006; Li, 2011; Zheng *et al.*, 2015; Wang *et al.*, 2016) and provided in Table 2.

Table 2. Material properties of Homogeneous and Nonhomogeneous models

Models		Young's Modulus (MPa)	Poisson's Ratio	Reference
Nonhomogeneous	Cortical	12,000	0.3	(Li and Wang, 2006; Zheng *et al.*, 2015)
	Trabecular	100	0.2	
	Nucleus pulposus	1	0.4999	
	Annular fibrosus	4.2	0.45	
Homogeneous	Bone	200	0.3	(Li, 2011; Wang *et al.*, 2016)
	Disc	4	0.4999	

All the connections were set to multi point constraint contact formulation. The solver type was set to direct. The large deflection was turned off and sub steps were added for gradual loading. By fixing the inferior surface of the vertebral body in the bottom part of the vertebra and applying a force of 1000 N on the superior surface of the vertebral body in the top vertebra, boundary conditions were added (refer to Figure 2). A force of 1000 N was selected because it was estimated that the lumbar spine receives a compressive load of 1000 N during standing and walking (Arjmand *et al.*, 2015). Five different simulations were performed on each L_1-L_2, L_2-L_3, L_3-L_4, and L_4-L_5 lumbar segments.

Due to the application of force on the lumbar finite element model, changes like stress, strain, and deformation were developed. The normal stress is computed as:

$$\{\sigma\} = [D]\{\varepsilon^{el}\} \tag{1}$$

Where, $\{\sigma\}$ is stress vector, $[D]$ is elasticity or elastic stiffness or stress strain matrix, $\{\varepsilon^{el}\} = \{\varepsilon\} - \{\varepsilon^{th}\}$ is elastic strain vector, $\{\varepsilon\}$ is total strain vector, and $\{\varepsilon^{th}\}$ is the thermal strain vector. While the strain is computed as:

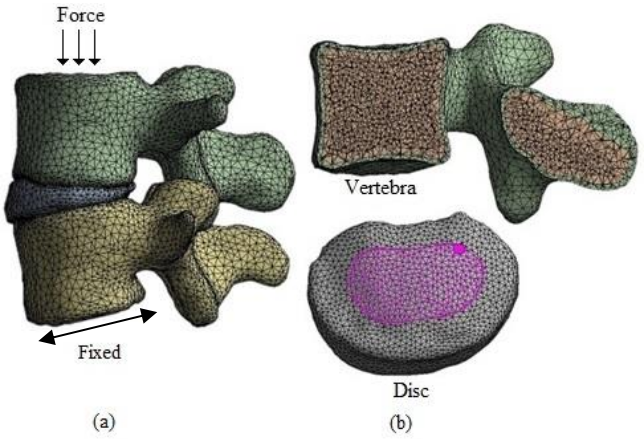

Figure 2. Lumbar finite element model. (a) Homogeneous model, (b) Nonhomogeneous model

$$\{\varepsilon\} = [B]\{u\} \tag{2}$$

Where, $[B]$ is the strain displacement matrix based on element shape, and $\{u\}$ is the nodal displacement vector. The deformation caused due to applied force is computed as:

$$\{u\} = \{x\} - \{X\} \tag{3}$$

Where, $\{u\}$ is displacement vector, $\{x\}$ is deformed, and $\{X\}$ is undeformed. The overall stress of a FE model is calculated as equivalent or von-Mises stress. It is computed as:

$$\varepsilon_e = \frac{1}{1+v'}\left(\frac{1}{2}[(\varepsilon_1 - \varepsilon_2)^2 + (\varepsilon_2 - \varepsilon_3)^2 + (\varepsilon_3 - \varepsilon_1)^2]\right)^{\frac{1}{2}} \tag{4}$$

Where, v' is effective Poisson's ratio. Whereas, the von-Mises strain of the FE model is computed as:

$$\varepsilon_{eq} = \frac{1}{\sqrt{2}(1+v)}\Big[(\varepsilon_x - \varepsilon_y)^2 + \left(\varepsilon_y - \varepsilon_z\right)^2 + (\varepsilon_z - \varepsilon_x)^2 + \frac{3}{2}\left(\gamma_{xy}^2 + \gamma_{yz}^2 + \gamma_{xz}^2\right)\Big]^{\frac{1}{2}} \tag{5}$$

Where, $\varepsilon_x, \varepsilon_y, \varepsilon_z$ is appropriate component strain values. The flexibility of a model in the finite element method is defined as:

$$[D]^{-1} = \begin{bmatrix} 1/E_x & -v_{xy}/E_x & -v_{xz}/E_x & 0 & 0 & 0 \\ -v_{yx}/E_y & 1/E_y & -v_{yz}/E_y & 0 & 0 & 0 \\ -v_{zx}/E_z & -v_{zy}/E_z & 1/E_z & 0 & 0 & 0 \\ 0 & 0 & 0 & 1/G_{xy} & 0 & 0 \\ 0 & 0 & 0 & 0 & 1/G_{yz} & 0 \\ 0 & 0 & 0 & 0 & 0 & 1/G_{xz} \end{bmatrix} \tag{6}$$

Where, E_x is Young's modulus in the X direction, v_{xy} is major Poisson's ratio, v_{yx} is minor Poisson's ratio, and G_{xy} is shear modulus in XY plane. Whereas, isotropic materials without shear moduli G_{xy}, G_{yz}, and G_{xz} are computed as:

$$G_{xy} = G_{yz} = G_{xz} = \frac{E_x}{2(1+v_{xy})} \tag{7}$$

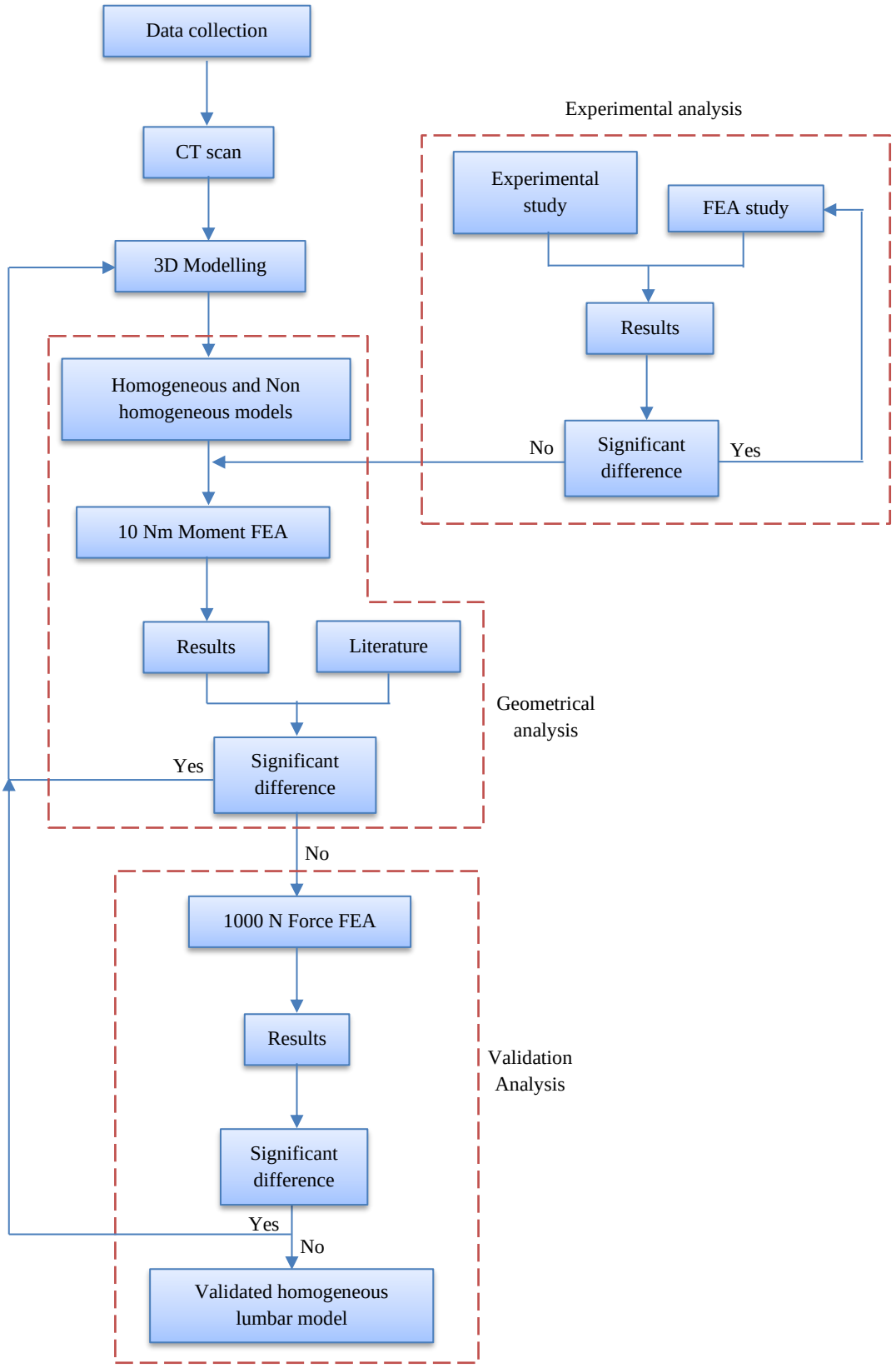

Figure 3. Flowchart of this study

Total lumbar segment strain and deformation, IVD stress, strain, and deformation were measured. Total deformation and total strain tools were used to find the deformation and strain of the whole lumbar model. Probes like deformation, stress, and strain were used to measure the deformation, stress, and strain of the IVD. A deformation probe was applied to the circumference of the IVD. Stress and strain probes were applied to the whole IVD. In this analysis, deformation is measured in millimetre (mm), stress in megapascal (MPa), and strain in millimetre per millimetre (mm/mm). On the subject of stress and strain, von Mises was measured. As the IVD can get expanded in all the X, Y, and Z-axis, for deformation, instead of selecting a particular axis, the sum of all was selected. The flowchart of this whole study is presented in Figure 3.

III. RESULT AND DISCUSSION

It took nearly three hours to simulate the non-homogeneous models and lesser for homogeneous models in a computer with a 5th generation intel i7 processor and 16 GB RAM. Table 3 and 4 display the results of disc stress, strain, and deformation, total strain, and deformation in lumbar segments between nonhomogeneous and homogeneous models under 1000 N force. The difference between homogeneous and nonhomogeneous models ranges between 0.92 to 1.25 MPa in disc stress, 0.30 to 0.43 mm/mm in disc strain, 0.44 to 0.91 mm in disc deformation, 0.31 to 0.41 mm/mm in total strain, and 0.45 to 0.91 mm in total deformation. With the overall 20 parameters mentioned below in Table 3 and 4, only 2 parameters under disc stress in $L_2 – L_3$ and $L_4 – L_5$ segments show a difference of more than 1 MPa, but lesser than 1.3 MPa. The remaining 18 parameters showed a difference of less than 1 MPa, mm, and mm/mm. Overall, the percentage difference may seem high. But the direct difference based on the numerical value is less.

The lumbar and cervical curvature are generally 'C' shaped when viewed in the sagittal plane. When a single lumbar or cervical segment is viewed alone with an imaginary line running parallel to the superior surface of the top vertebra and inferior surface of the bottom vertebra, it looks like a wedge-shaped and the IVD typically looks like a wedge (refer to Figure 4). This happens because the anterior lumbar IVD height is always higher than the posterior lumbar IVD (Hong *et al.*, 2010; Mirab *et al.*, 2017). The contour plots of lumbar IVD in this study showed mild contour difference between homogeneous and nonhomogeneous models because of the difference in geometrical type and the assigned material properties.

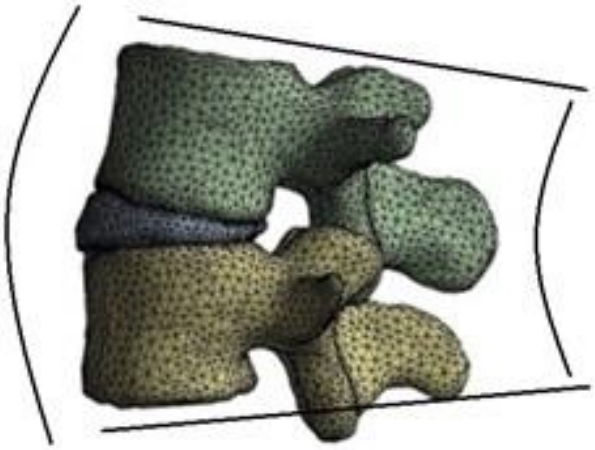

Figure 4. Wedge-shaped lumbar vertebral segment

Figure 5 represents the contour plots of von Mises stress, strain, and total deformation of the lumbar IVD under 1000 N of force. From these contour plots, it can be inferred that, while applying force, due to the wedge shape of IVD, 'C' shaped vertebral segment, and height of facet joints, the posterior or postro-lateral part of the IVD reacts more. The total deformation of homogeneous IVD in $L_1 – L_2$ is 0.52 mm, L_2-L_3 is 0.76 mm, L_3-L_4 is 0.55 mm, L_4-L_5 is 0.72 mm. Whilst, the total deformation of nonhomogeneous IVD in $L_1 – L_2$ is 1.22 mm, L_2-L_3 is 1.67 mm, L_3-L_4 is 1 mm, L_4-L_5 is 1.59 mm. Due to the layers of IVD, a noticeable difference was seen in the contour plot of IVD total strain. The total strain of homogeneous IVD in $L_1 – L_2$ is 0.05 mm/mm, L_2-L_3 is 0.04 mm/mm, L_3-L_4 is 0.05 mm/mm, L_4-L_5 is 0.04 mm/mm. Whereas, the total strain of nonhomogeneous IVD in $L_1 – L_2$ is 0.41 mm/mm, L_2-L_3 is 0.45 mm/mm, L_3-L_4 is 0.36 mm/mm, L_4-L_5 is 0.43 mm/mm. There were no visible or evident changes in the contour plots of homogeneous and nonhomogeneous IVD total stress.

In the present study, the IVD deformation of L_3-L_4 nonhonogeneous model was found to be 0.96 mm. Another

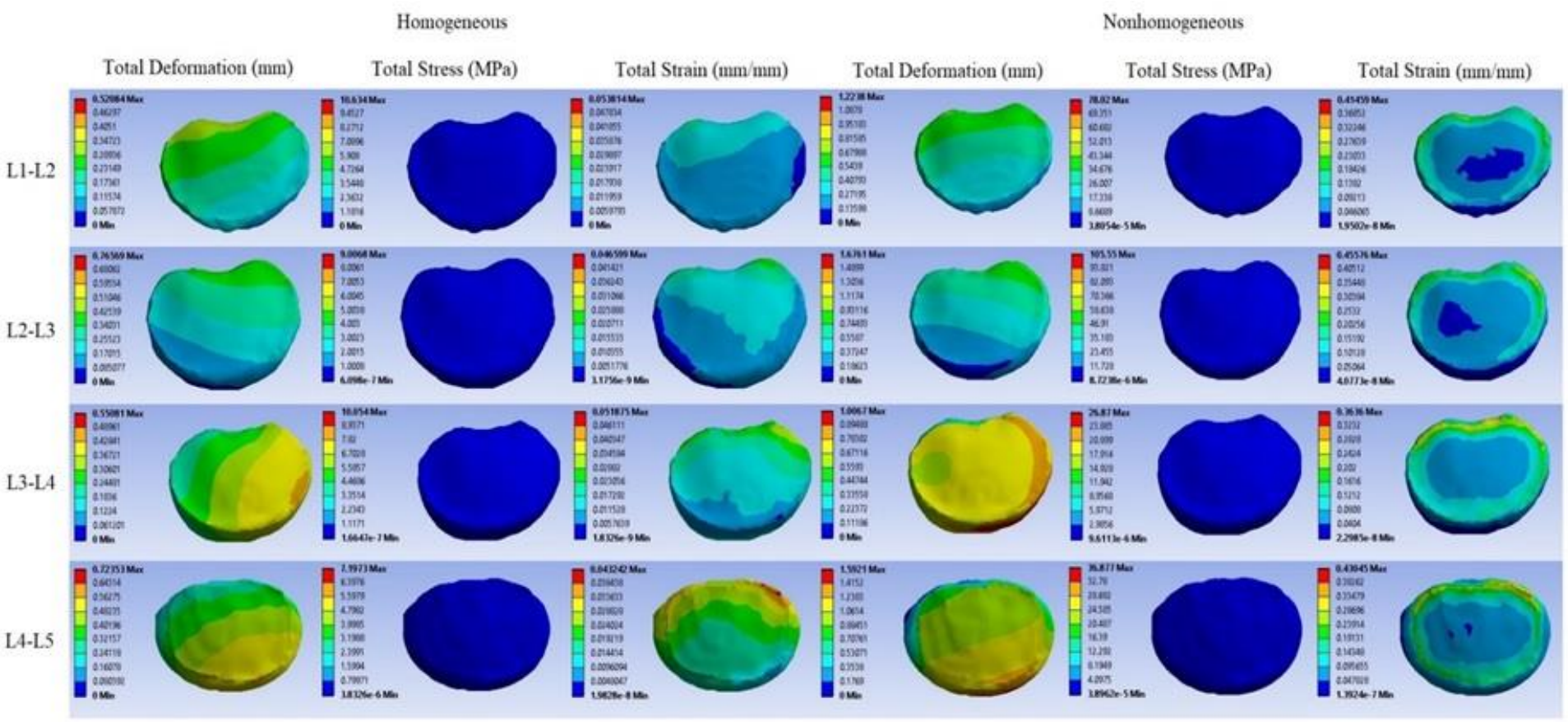

Figure 5. Contour images of IVD under total stress, strain, and deformation between Homogeneous and Nonhomogeneous model

Table 3. Results of the Intervertebral disc

Segment	Disc stress (MPa)				Disc strain (mm/mm)				Disc deformation (mm)			
	NH	H	Difference	% Difference	NH	H	Difference	% Difference	NH	H	Difference	% Difference
$L_1 – L_2$	1.03	0.09	0.94	91.26	0.34	0.02	0.32	94.11	0.76	0.32	0.44	57.89
$L_2 – L_3$	1.34	0.09	1.25	93.28	0.45	0.02	0.43	95.55	0.87	0.40	0.47	54.02
$L_3 – L_4$	1.07	0.15	0.92	85.98	0.33	0.03	0.30	90.90	0.96	0.44	0.52	54.16
$L_4 – L_5$	1.41	0.17	1.24	87.94	0.43	0.04	0.39	90.69	1.48	0.57	0.91	61.48

NH – Nonhomogeneous, H - Homogeneous

Table 4. Results of the whole lumbar segment

Segment	Total strain (mm/mm)				Total deformation (mm)			
	NH	H	Difference	% Difference	NH	H	Difference	% Difference
$L_1 – L_2$	0.41	0.05	0.36	87.80	1.22	0.52	0.70	57.37
$L_2 – L_3$	0.45	0.04	0.41	91.11	1.67	0.76	0.91	54.49
$L_3 – L_4$	0.36	0.05	0.31	86.11	1	0.55	0.45	45.00
$L_4 – L_5$	0.43	0.04	0.39	90.69	1.59	0.72	0.87	54.71

finite element model study on L_3-L_4 lumbar vertebrae reported that the deformation on L_3-L_4 IVD under 1200 N of compression was to be 0.9 mm (Coogan *et.al.*, 2016). This difference could be due to the finite element models used in the respective studies. Coogan *et.al.*, used the CT images of cadavers with a mean age of 42.2 ± 13.7 years. Their finite element model included the cartilaginous endplate and cortical bone with shell elements. Vertebrae were meshed with four node tetrahedral elements, their IVD was meshed with eight node hexahedral elements, and used isotropic material properties for their model.

Another FEA study (Li and Wang, 2006) on lumbar disc biomechanical analysis which used an isotropic $L_1 – L_2$ segment of a young adult reported that the total deformation of $L_1 – L_2$ segment under 1000 N of the axial load was 0.8 mm. Whereas, in the present study, the total deformation of $L_1 – L_2$ segment is 0.52 mm. The reported disc stress and deformation of $L_1 – L_2$ segment cadaver experimental results under 1000 N of pressure in the age group of 22 to 77 years old was found to be 0.74 ± 0.15 MPa and 0.4 ± 0.2 mm (O'Connell *et al.*, 2007). The disc pressure of 0.74 MPa may seem quite higher than 0.09 MPa. It is because, the lumbar segments used by O'Connell *et al.*, had their posterior facets removed and only the vertebral body was used. Hence, there is no obstruction or limitation in their axial compression. Moreover, cadaver discs have low fluid and nutrition levels. But, it should be noted that the normal IVDs have an intrinsic pressure of approximately 0.7 kg/cm^2 or 0.0686 Mpa, even when they are unloaded. When the vertical load is applied to the disc, the pressure in the nucleus is 50% higher than that applied externally. Despite the percentage difference between homogeneous and nonhomogeneous models, the results of IVD stress and IVD deformation from this study are within the range of data reported in the experimental studies.

There were a few limitations to this study. Eventhough the hexahedral elements provide more accuracy, this study used tetrahedral elements. The software which was used to develop 3D models of vertebrae and IVD has no option to export in hexahedral. There was no literature study supporting the idea of converting a tetrahedral into a hexahedral using additional software. Whereas, several studies used tetrahedral elements (Wang *et.al.*, 2016; Meng *et.al.*, 2013; Jaramillo *et.al.*, 2015). The second limitation would be the usage of isotropic material properties. Bone is generally considered as nonhomogeneous and anisotropic in nature. This study used homogeneous models to validate, and there were no data found in the literature, using anisotropic material properties in a homogeneous model. It shall be experimented in the future research.

IV. CONCLUSION

The direct comparison between homogeneous and nonhomogeneous models on disc stress, strain, deformation, total strain, and deformation showed a difference of less than one in terms of numerical value in most of the data collected. But in terms of percentage, the difference is high. Hence, considering bone and disc which are nonhomogeneous in nature as a homogeneous does not produce a significant difference in the given scenario. The observation of IVD mechanical forces was consistent with those reported in the literature for IVD stress and IVD deformation. This assumption of nonhomogeneous as the homogeneous model allows the researchers to utilize the artifact affected images, which results in helping the patients to achieve a healthy lifestyle. Therefore, the homogeneous lumbar vertebral segment used in this study is reliable, validated, and will be used for further more analysis. Additional studies are required to analyse the validity of assuming human lumbar vertebrae as homogeneous with multiple segments.

V. ACKNOWLEDGEMENT

A heartfelt thanks to Dr. Nalli R Yuvaraj, orthopaedic spine surgeon from Rajiv Gandhi Government General Hospital, Chennai, for his help and constant support during the data collection. Cordial thanks to Dr. Chin Seong Lim, faculty of engineering, University of Nottingham Malaysia, for his help and support in performing structural simulations at the University of Nottingham Malaysia.

Declarations

Funding

Not applicable.

Conflict of Interest

On behalf of all authors, the corresponding author states that there is no conflict of interest.

Availability of data

Data sharing not applicable – no new data generated.

VI. REFERENCES

Arjmand, N, Amini, M, Shirazi-Adl, A, Plamondon, A & Parnianpour, M 2015, 'Revised NIOSH lifting equation may generate spine loads exceeding recommended limits', International Journal of Industrial Ergonomics, vol. 47, pp. 1-8.

Bisschop, A, van Dieen, JH, Kingma, I, van der Veen, AJ, Jiya, TU, Mullender, MG, Paul, CPL, de Kleuver, M & van Royen, BJ 2013, 'Torsion biomechanics of the spine following lumbar laminectomy: a human cadaver study', European Spine Journal, vol. 22, no. 8, pp. 1785-1793.

Coogan, JS, Francis, WL, Eliason, TD, Bredbenner, TL, Stemper, BD, Yoganandan, N, Pintar, FA & Nicolella DP 2016, 'Finite Element Study of a Lumbar Intervertebral Disc Nucleus Replacement Device', Frontiers in Bioengineering and Biotechnology, vol. 4, pp. 1-11.

Doulgeris, JJ, Gonzalez-Blohm, SA, Aghayev, K, Shea, TM, Lee, WE, Hess, DP & Vrionis, FD 2014, 'Axial rotation mechanics in a cadaveric lumbar spine model: a biomechanical analysis', The Spine Journal, vol. 14, no. 7, pp. 1272-1279.

Erwin, WM & Hood, Katherine 2014, 'The cellular and molecular biology of the intervertebral disc: A clinician's primer', The Journal of the Canadian Chiropractic Association, vol. 58, no. 3, pp. 246-257.

Eswaran, SK, Gupta, A & Keaveny, TM 2007, 'Locations of bone tissue at high risk of initial failure during compressive loading of the human vertebral body', Bone, vol. 41, no. 4, pp. 733-739.

Hong, CH, Park, JS, Jung, KJ & Kim, WJ 2010, 'Measurement of the normal lumbar intervertebral disc space using magnetic resonance imaging', Asian Spine Journal, vol. 4, no. 1, pp. 1-6.

Hutton, W, Cyron, B & Stott, J 1979, 'The compressive strength of lumbar vertebrae', Journal of Anatomy, vol. 129,

no. 4, pp. 753-758.

Jaramillo, HE, Gomez, L & Garcia, JJ 2015, 'A finite element model of the L_4-L_5-S_1 human spine segment including the heterogeneity and anisotropy of the discs', Acta of Bioengineering and Biomechanics, vol. 17, no. 2, pp. 15-24.

Jones, AD 2013, Biomechanical and finite element analyses of alternative cements for use in vertebral kyphoplasty, The University of Toledo Digital Repository, viewed 16 July 2019, <https://etd.ohiolink.edu/pg_10?0::NO:10:P10_ACCESSION_NUM:toledo1364828764>.

Li, H 2011, 'An approach to lumbar vertebra biomechanical analysis using the finite element modeling based on CT images', eds N Homma, in Theory and Applications of CT Imaging and Analysis, Rijeka, pp. 165-180.

Li, H & Wang, Z 2006, 'Intervertebral disc biomechanical analysis using the finite element modeling based on medical images', Computerized Medical Imaging and Graphics, vol. 30, no. 6-7, pp. 363-370.

Meng, L, Zhang, Y & Lu, Y 2013, 'Three-dimensional finite element analysis of mini-external fixation and Kirschner wire internal fixation in Bennett fracture treatment', Orthopaedics & Traumatology: Surgery & Research, vol. 99, pp. 21-29.

Mirab, SM, Barbarestani, M, Tabatabaei, SM, Shahsavari, S & Zangi, MB 2017, 'Measuring dimensions of lumbar intervertebral discs in normal subjects', Anatomical Sciences, vol. 14, no. 1, pp. 3-8.

Oatis, CA (eds) 2016, Kinesiology: The mechanics and pathomechanics of human movement, 3rd edn, Lippincott Williams & Wilkins, Philadelphia, USA.

O'Connell, GD, Johannessen, W, Vresilovic, EJ & Elliott, DM 2007, 'Human internal disc strains in axial compression measured noninvasively using magnetic resonance imaging', Spine, vol. 32, no. 25, pp. 2860-2868.

Palaniswamy, M, Shuib, AS, Ching, K, Koshy, S, Chinna, K & Seong CL 2019, 'Validation of finite element model of human lumbar vertebrae under mechanical forces', in 12th EURECA International Engineering Research Conference: AIP Conference Proceedings, Kuala Lumpur, 3rd & 4th July 2019, Kuala Lumpur.

Pianykh, O (eds) 2012, Digital Imaging and Communications in Medicine (DICOM), 2nd edn, Springer, Berlin, Germany.

Rahm, MD, Brooks, DM, Harris, JA, Hart, RA, Hughes, JL, Ferrick, BJ & Bucklen, BS 2019, 'Stabilizing effect of the rib cage on adjacent segment motion following thoracolumbar posterior fixation of the human thoracic cadaveric spine: A biomechanical study', Clinical Biomechanics, vol. 70, pp. 217-222.

Shamnadh, M, Aravind, C & Dileep, PN 2017, 'CT based finite element analysis of human lumbar vertebra with accurate geometric and material property assumptions', International Journal of Scientific & Engineering Research, vol. 8, no. 7, pp. 121-125.

Trexler, MM, Lennon, AM, Wickwire, AC, Harrigan, TP, Luong, QT, Graham, JL, Maisano, AJ, Roberts, JC & Merkle, AC 2011, 'Verification and implementation of a modified split hopkinson pressure bar technique for characterizing biological tissue and soft biostimulant materials under dynamic shaer loading', Journal of the Mechanical Behavior of Biomedical Materials, vol. 4, no. 8, pp. 1920-1928.

Wang, L, Zhang, B, Chen, S, Lu, X, Li, ZY & Guo, Q 2016, 'A validated finite element analysis of facet joint stress in degenerative lumbar scoliosis', World Neurosurgery, vol. 95, pp. 126-133.

Weerasooriya, T, Sanborn B, Gunnarsson, A & Foster, M 2016, 'Orientation Dependent Compressive Response of Human Femoral Cortical Bone as a Function of Strain Rate', Journal of Dynamic Behaviour of Materials, vol. 2, pp. 74-90.

Zheng, J, Yang, Y, Lou, S, Zhang, D & Liao, S 2015, 'Construction and validation of a three-dimensional finite element model of degenerative scoliosis', Journal of Orthopaedic Surgery and Research, vol. 10, no. 189, pp. 1-7.

Zulkifli, A, Ariffin, A & Rahman, M 2011, 'Probabilistic finite element analysis of vertebrae of the lumbar spine under hyperextension loading', International Journal of Automotive and Mechanical Engineering, vol. 3, pp. 256-264.